International Journal of Green Energy

ISSN: 1543-5075 (Print) 1543-5083 (Online) Journal homepage: www.tandfonline.com/journals/ljge20

Comprehensive comparison of global mechanisms for methane combustion optimized using artificial neural network

Shuang Li , Xiangtao Liu , Jicang Si , Guochang Wang , Yuanye Guo , Mengwei Wu , Enguang Xu , Minyi Xu & Jianchun Mi

To cite this article: Shuang Li , Xiangtao Liu , Jicang Si , Guochang Wang , Yuanye Guo , Mengwei Wu , Enguang Xu , Minyi Xu & Jianchun Mi (09 Jun 2025): Comprehensive comparison of global mechanisms for methane combustion optimized using artificial neural network, International Journal of Green Energy, DOI: 10.1080/15435075.2025.2516038

To link to this article: https://doi.org/10.1080/15435075.2025.2516038

Published online: 09 Jun 2025.

INTERNATIONAL JOURNAL OF GREEN ENERGY
https://doi.org/10.1080/15435075.2025.2516038

Taylor & Francis
Taylor & Francis Group

Comprehensive comparison of global mechanisms for methane combustion optimized using artificial neural network

Shuang Li[a], Xiangtao Liu[b], Jicang Si[a], Guochang Wang[c], Yuanye Guo[a], Mengwei Wu[a], Enguang Xu[d], Minyi Xu[a], and Jianchun Mi[b]

[a]Marine Engineering College, Dalian Maritime University, Dalian, P.R. China; [b]College of Engineering, Peking University, Beijing, P.R. China; [c]State Key Laboratory of Clean and Efficient Coal Utilization, Taiyuan University of Technology, Taiyuan, P.R. China; [d]Dalian Shipbuilding Industry Co., Ltd., Dalian, P.R. China

ABSTRACT

Global mechanisms significantly reduce computational costs in methane combustion simulations but their predictive accuracy and applicability are often limited due to the lack of validation across diverse combustion conditions. This study systematically evaluates various global mechanisms by comparing them to the detailed mechanism GRI-Mech 3.0 (abbreviated as GRI-3.0) under a range of temperature (1200 K–2500 K), oxygen concentrations (0.1–1), and mixing modes. All global mechanisms are first optimized using an artificial-neural-network (ANN)-based method to closely match GRI-3.0 in the perfectly stirred reactor (PSR). Their performances are tnen assessed in computational fluid dynamics (CFD) simulations of various combustion systems, including the open jet-in-hot-coflow (JHC) and in-furnace systems, under both non-premixed and premixed conditions. Results indicate that under non-premixed conditions, the global mechanism proposed by Si et al. (***Energy & Fuels***, 2021, 35(18), 14941-14953.) performs best ($RE_{CO,averaged} = 0.179$, $RE_{T,averaged} = 0.137$), and the reaction $CH_4+H_2O \rightarrow CO+3H_2$ leads to an overestimation of X_{CO}. Under premixed conditions, the mechanism proposed by Jones & Lindstedt (***Combust Flame***, 1988, 73(1), 233–249.) more accurately predicts CO distribution ($RE_{CO,averaged} = 0.354$), highlighting the critical role of the reaction $CH_4+H_2O \rightarrow CO+3H_2$ in converting intermediate CO and the reaction $CO+0.5O_2 \leftrightarrow CO_2$ leads to inaccurate CO conversion.

ARTICLE HISTORY
Received 9 March 2025
Accepted 31 May 2025

KEYWORDS
Global mechanism; optimization; artificial neural network (ANN); computational fluid dynamics (CFD); premixed & non-premixed flame

Introduction

The combustion of fossil fuels is a crucial energy source but produces various pollutants, such as CO_2 and NO_x, which pose significant risks to human society. To improve efficiency and reduce emissions of combustion, a number of advanced technologies, including oxy-fuel combustion (Li et al. 2021; Liu et al. 2022) moderate and intense low-oxygen dilution (MILD) combustion (Kuang et al. 2022; Xu et al. 2024) staged combustion (Li, Zhang, and Zhang 2024; Zhang et al. 2023) lean-fuel combustion (Dunn-Rankin 2011; Fursenko et al. 2020) and chemical-looping combustion (Normann et al. 2019) have been developed. Each of those technologies operates under specific conditions: for instance, staged combustion separates the combustion process into a fuel-rich region and a fuel-lean region, while MILD combustion uses reduced oxygen levels.

Computational fluid dynamics (CFD) is an important tool for analyzing combustion and emissions characteristics. Techniques such as direct numerical simulation (DNS) (Kiran et al. 2023; Lamioni et al. 2020; Minamoto and Swaminathan 2014) large eddy simulation (LES) (Wang and Mi 2018; Xiong et al. 2020) and Reynolds-averaged Navier – Stokes (RANS) (Manzoor et al. 2024; Zivkovic and Sattelmayer 2023) are employed to study combustion processes across different temporal and spatial scales. However, using detailed reaction mechanisms such as GRI-Mech-3.0 (Smith et al. 1999) in DNS and LES is computationally intensive, or even impossible. As shown in Table 1, prior studies (Doan and Swaminathan 2019; Harvazinski, Talley, and Sankaran 2016; Minamoto and Swaminathan 2014; Si et al. 2020) indicate that the computational cost increases substantially with the number of reactions in a chemical mechanism, particularly in DNS and LES. Therefore, for studies that do not require detailed tracking of intermediate species and complex reaction processes, global mechanisms that include only major species can effectively balance the predicting accuracy with the computational efficiency.

The global mechanisms by Jones & Lindstedt (Jones and Lindstedt 1988) (JL) and Westbrook & Dryer (Westbrook and Dryer 1981) (WD) are the primary choices for CH_4 combustion. Compared to the JL mechanism, the WD mechanism lacks the reaction that converts CO to CO_2, which reduces its accuracy in predicting CO levels during combustion (Si et al. 2021). In contrast, the JL mechanism includes four key reactions that well describe the conversion of CH_4 into CO and H_2, and subsequently into the final products (CO_2 and H_2O), as outlined below:

$$CH_4 + 0.5O_2 \rightarrow CO + 2H_2 \quad (1)$$

CONTACT Jicang Si sjc@dlmu.edu.cn Marine Engineering College, Dalian Maritime University, Dalian 116026, P.R. China

Table 1. Calculation cost in previous CFD studies.

Researcher	Model	Grid number	Reaction number	Mechanism type	Core hours
Si et al. (2020)	RANS	300,000	4	Global Jones and Lindstedt (1988)	448
	RANS	300,000	325	Detail Smith et al. (1999)	1960
	RANS	40,000	4	Global Jones and Lindstedt (1988)	5.6
	RANS	40,000	325	Detail Smith et al. (1999)	14
Harvazinski, Talley, and Sankaran (2016)	LES	4,000,000	1	Global Westbrook and Dryer (1981)	230,400
	LES	4,000,000	177	Detail Frenklach et al. (1995)	5,184,000
Minamoto and Swaminathan (2014)	DNS	134,217,728	36	Smooke (1991)	490,000
Doan and Swaminathan (2019)	DNS	134,217,728	58	Doan, Swaminathan, and Minamoto (2018)	2,252,800

$$CH_4 + H_2O \rightarrow CO + 3H_2 \tag{2}$$

$$CO + H_2O \leftrightarrow CO_2 + H_2 \tag{3}$$

$$H_2 + 0.5O_2 \leftrightarrow H_2O \tag{4}$$

For a given reaction A + B → C + D, the chemical reaction rate (v) can be determined by

$$v = -k[A]^m[B]^n \tag{5}$$

where m and n are the reaction orders and [A] and [B] are the mole fraction of species A and B. The chemical reaction rate constant (k) can be expressed using the Arrhenius equation (Turns 1996):

$$k = AT^b e^{\frac{-E_a}{RT}} \tag{6}$$

where T is the temperature, A is the pre-exponential factor, b is the temperature exponent, E_a is the activation energy, and R is the ideal gas constant.

The study of Jones and Lindstedt (Jones and Lindstedt 1988) demonstrated the effectiveness of the JL mechanism in simulating counterflow flames. Later, Meredith and Black (Meredith and Black 2006) introduced a new global mechanism for CH_4-air combustion in perfectly stirred reactor (PSR), referred to as M3–1 in Table 2, with specific reactions detailed in Table 3. They found that the M3–1 mechanism outperformed the WD mechanism in predicting both adiabatic flame temperature and species concentrations. Abou-Taouk et al. (Abou-Taouk et al. 2013) introduced the M4–1 mechanism and compared its performance to the WD and JL mechanisms, finding that M4–1 performed best in predicting laminar flame speed and exhaust gas concentrations.

However, A. Frassoldati et al. (Frassoldati et al. 2008) highlight the temperature peaks of $CH_4/O_2/N_2$ combustion limit the validity of JL mechanism and WD mechanism. Consequently, to improve the accuracy of combustion simulations, optimizing the Arrhenius parameters (A, b, and E_a) is necessary for various combustion systems. Specifically, in MILD combustion condition, Kim et al. (Kim, Schnell, and Scheffknecht 2008) optimized R6 (see Table 3) in the JL mechanism with parameters from Marinov et al. (Marinov and Westbrook 1996) which improved the predictions of CO distribution. Subsequent studies by Wang et al. (Wang et al. 2012) and Tu et al. (Tu, Yang, and Liu 2017) also optimized R6 of the JL and WD mechanisms in open and closed MILD combustion systems, respectively. Both studies found that the WD

Table 2. Components of global mechanisms in the present study.

Mechanism name	Number of reactions	Reactions involved	Combustion mode
M3–1 (Li, Zhang, and Zhang 2024)	3	R1, R5, R6	Conventional air combustion
M3–2	3	R1, R4, R6	/
M4–1 (Liu et al. 2022)	4	R1, R4, R5, R6	Conventional air combustion
M4–2	4	R1, R3, R5, R6	/
M4–3	4	R1, R3, R4, R6	/
Jones and Lindstedt (1988)	4	R1, R2, R4, R6	Conventional air combustion, MILD combustion, Oxy combustion
GM (Li et al. 2021)	4	R1*, R4, R5*, R6	MILD combustion
M5–1	5	R1, R2, R4, R5, R6	/
M5–2	5	R1, R3, R4, R5, R6	/
M5–3	5	R1, R2, R3, R5, R6	/
M5–4	5	R1, R2, R3, R4, R6	/
M6	6	R1, R2, R3, R4, R5, R6	/

Table 3. Global reactions for CH_4 combustion.

Reaction No.	Reactions	Reaction order
R1	$CH_4 + 0.5\ O_2 \rightarrow CO + 2\ H_2$	$[CH_4]^{0.5}[O_2]^{1.25}$
R1 (Li et al. 2021)	$CH_4 + 0.5\ O_2 \rightarrow CO + 2\ H_2$	$[CH_4][O_2]^{0.5}$
R2	$CH_4 + H_2O \rightarrow CO + 3\ H_2$	$[CH_4][H_2O]$
R3	$CH_4 + CO_2 \rightarrow 2\ CO + 2\ H_2$	$[CH_4][CO_2]$
R4	$CO + H_2O \rightleftharpoons CO_2 + H_2$	$[CO][H_2O]$
R5	$CO + 0.5\ O_2 \rightleftharpoons CO_2$	$[CO][O_2]^{0.25}[H_2O]^{0.5}$
R5 (Li et al. 2021)	$CO + 0.5\ O_2 \rightleftharpoons CO_2$	$[CO][O_2]^{0.5}$
R6	$H_2 + 0.5\ O_2 \rightleftharpoons H_2O$	$[H_2][O_2]^{0.5}$

mechanism provided a better description of CH_4 oxidation rates. However, the JL and WD mechanisms tended to overestimate and underestimate CO production, respectively. Anderson et al. (Andersen et al. 2009) observed similar results in non-premixed oxy-combustion systems. Moreover, parameter optimization for the JL mechanism was also conducted in $CH_4/O_2/N_2$ (Frassoldati et al. 2008) and $CH_4/O_2/CO_2$ (Hu et al. 2018) combustion systems.

Recently, Si et al. (Si et al. 2020) proposed an artificial neural network (ANN)-based method to optimize the Arrhenius parameters of the JL mechanism under MILD combustion regime. Their study demonstrated that the prediction accuracy of the ANN-optimized mechanism significantly surpassed that of other modified JL mechanisms from previous studies (Hu et al. 2018; Jones and Lindstedt 1988; Kim, Schnell, and Scheffknecht 2008; Wang et al. 2012). However, discrepancies in CO distribution persisted in non-premixed MILD combustion, primarily due to the overestimation of CO consumption in R4 on the fuel-lean side. To address this issue, they proposed a new global mechanism named as GM [26], as shown in Table 2. Comparative analyses showed that CFD simulations using the GM mechanism were more accurate than those using the modified JL, WD, or a combination of reactions from both the JL and WD mechanisms.

However, previous studies have only investigated a limited number of global mechanisms under specific reaction conditions (as summarized in Table 2). To our best knowledge, a systematic and comprehensive comparison of all major global mechanisms across a broad range of combustion conditions has not been conducted. Consequently, the applicability of these mechanisms under diverse operating conditions – such as varying temperatures, oxygen concentrations, and reactant mixing modes – remains largely undetermined.

To address the aforementioned research gaps, the present study employs an ANN-based optimization framework to refine the existing global mechanisms in perfectly PSR simulations across different temperatures and O_2 concentrations. The optimized mechanisms are further validated through comprehensive CFD simulations encompassing both premixed and non-premixed mixing modes, as well as different combustion configurations including open and closed systems, under diverse operating conditions.

The objective of this study is to provide a systematic and quantitative evaluation of the predictive performance of each global mechanism. Specifically, it seeks to address the following two fundamental research questions:

(1) Which global mechanism demonstrates the highest predictive accuracy under significantly varying combustion conditions?
(2) What are the dominant factors and reaction characteristics that govern the accuracy of global mechanisms across different combustion environments?

Computational scheme

Simulated combustion systems

The PSR model in CHEMKIN-Pro 18.0 (ANSYS Fluent 2017) software is utilized in this study to optimize the parameters of the global mechanisms. This model assumes complete mixing of fuel and oxidant before their reactions, thus effectively neglecting the effects of mixing, convection, and radiation. A transient solver with a residence time of 1.0 sec is used in the simulations. Specific details regarding the temperature and reactant concentrations in the PSR cases are provided in Table 4.

The performance of different global mechanisms is then validated through CFD simulations across multiple combustion systems, including both open and closed configurations, as well as premixed and non-premixed modes, as illustrated in Figure 1. Note that NP-JHC and P-JHC represent non-premixed and premixed open jet flames, respectively (Dally, Karpetis, and Barlow 2002) (Figure 1(a,b)). The NP-JHC configuration contains a central fuel jet with a diameter of 4.25 mm and a coaxial hot coflow with a diameter of 82 mm. For the P-JHC configuration, the premixed reactant is injected from the central jet, which has a diameter of 4.25 mm, while the coflow consists of N_2. Moreover, for both open systems, outside is the ambient air. Two-dimensional (2D) computational domains are employed for the simulations due to the axial symmetry of the combustion system. Figure 1 provides the mesh details of the computational domain after grid independence verification.

Additionally, two closed combustion systems are used in this study: the non-premixed furnace (NPF) (Si et al. 2021) and the premixed furnace (PF) (Shu et al. 2020) systems (Figure 1). Both systems share an identical furnace with a diameter of 300 mm and a length of 1200 mm, with the burner located at the bottom. In the NPF system, the burner consists of a 3.5 mm diameter fuel jet and a coaxial annular oxidizer jet with inner and outer diameters of 26.5 mm and 29.5 mm, respectively. In contrast, the PF system uses a burner with a premixed jet of 10.61 mm in diameter. In these combustion systems,

Table 4. Simulation conditions for the PSR, NP-JHC, P-JHC, NPF, and PF combustion systems. f_M represents the mole fraction of species M, Φ is the equivalent ratio.

Case	Fuel	Oxidant		Φ	T_{PSR} (T_{coflow}, T_{wall})/K	P/kW
	f_{CH4}	f_{O2}	f_{N2}			
PSR	1	0.1–1	0.9–0	1	1200, 1800, 2500	–
NP-JHC Dally, Karpetis, and Barlow (2002)	1	0.1–1	0.9–0		1200, 1800, 2500	40
P-JHC	1	0.1–1	0.9–0		1200, 1800, 2500	12
NPF Si et al. (2021)	1	0.1–1	0.9–0	0.9	1200, 1800, 2500	25
PF Shu et al. (2020)	1	0.1–1	0.9–0	0.9	1200, 1800, 2500	25

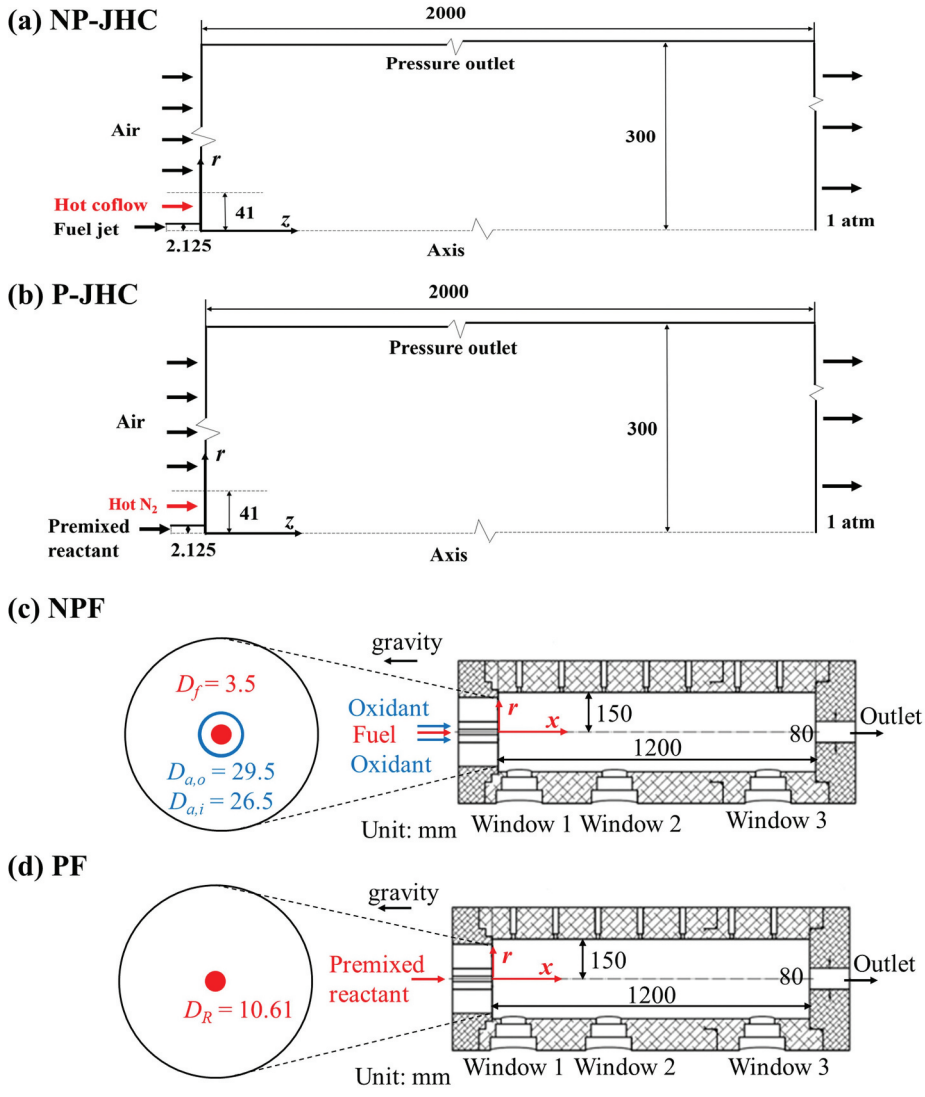

Case	Mesh Dimension	Number of grids	Minimum grid size/mm^3
NP-JHC/P-JHC	2D	40,000	4.52×10^{-2} mm^2
NPF	2D	52,000	2.50×10^{-1} mm^2
PF	2D	50,000	5.25×10^{-1} mm^2

Figure 1. Computational domain for the (a) NP-JHC, (b) P-JHC, (c) NPF, and (d) PF systems. Units are mm.

simulations are conducted using 2D computational domains. Previous studies (Galletti, Parente, and Tognotti 2007; Shu et al. 2020; Si et al. 2021) have shown that for axisymmetric configurations, 2D simulations perform comparably to 3D simulations. Detailed information on the fuel-oxidizer composition and grid details for the NPF and PF systems is provided in Figure 1.

The commercial CFD software ANSYS Fluent 2022R1 (ANSYS® Fluent 2022) is used in this study. The modified k–ε model (Pope 1978) (with the model parameter $C_{1\varepsilon}$ changing from 1.44 to 1.60) is employed to simulate turbulent flow. The eddy dissipation concept (EDC) model (Di et al. 2022; Farokhi and Birouk 2020; Magnussen 1981; Putra and Ertesvåg 2023) is applied to solve turbulence–chemistry interactions. Additionally, the discrete ordinate (DO) model (Amini et al. 2023; Chui and Raithby 1993; Sarr, Groth, and Hu 2019) together with the weighted sum of gray gas (WSGG) (Rodrigues et al. 2019) model is adopted as radiation models. To improve the accuracy of the numerical solution, the quadratic upwind interpolation for convection kinetics (QUICK) scheme is chosen. Note that these models have been extensively validated in previous studies on JHC

(Christo and Dally 2005; Hu et al. 2018; Kim, Schnell, and Scheffknecht 2008; Si et al. 2020, 2021; Wang et al. 2012) NPF (Si et al. 2021) and PF (Shu et al. 2020) combustion systems.

ANN-based parameter optimization method

Previous studies (Frassoldati et al. 2008; Si et al. 2021; Tu, Yang, and Liu 2017) have highlighted the importance of optimizing the reaction parameters of global mechanisms under varying conditions, such as, O_2 concentration (f_{O2}) and temperature (T). To effectively optimize the parameters, we employed a method based on artificial neural networks (ANN), as proposed in our earlier study (Si et al. 2020). Detailed information on the procedure, algorithm, and calculation time is available in that work (Si et al. 2020). Briefly, the ANN-based parameter optimization process involves three key steps, as illustrated in Figure 2:

Step 1: Generating training and testing datasets. For each reaction in the mechanism, Arrhenius parameters A and E_a are randomly generated from a uniform distribution to create 20,000 datasets for training and 10,000 datasets for validation. The parameter ranges of A and E_a are set as (10^9, 10^{15}) and (15000, 40000), respectively. Each parameter set is simulated in a perfectly stirred reactor (PSR) under specific f_{O2} and T_{PSR} conditions (f_{O2} = 0.1, 0.21, 0.3, 0.5, 0.75, and 1; T_{PSR} = 1200, 1800, and 2500 K, as shown in Table 2). The maximum and equilibrium mole fractions of CO ($X_{CO,max}$ and $X_{CO,equilibrium}$, respectively) are recorded as the training and validating outputs. Due to the relatively narrow temperature range for each

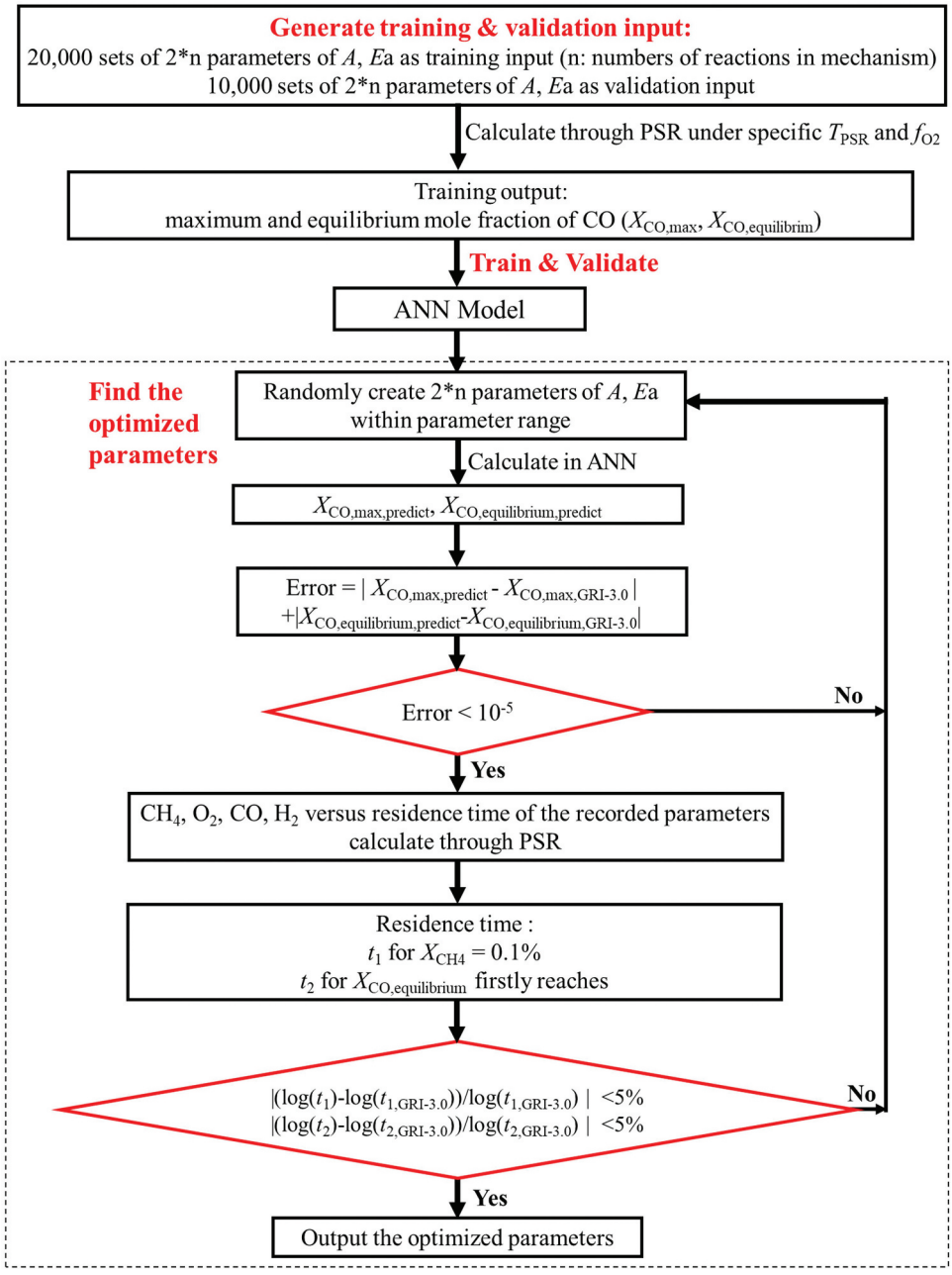

Figure 2. Algorithm for ANN-based parameter optimization (Si et al. 2021).

optimization (approximately ±300 K), only parameters A and E_a are selected, with the temperature exponent parameter b set to 0, which has proven to be sufficient based on the results.

Step 2: Train the ANN. MATLAB R (2023a) is applied for ANN construction and training, followed by parameter optimization.

Step 3: Determine the optimal parameters from the ANN. The optimized parameters are verified by evaluating the residence times required for complete CH_4 consumption and peak X_{CO} value. The optimized parameters can be found in the Supplementary Material, and the optimized global mechanisms are referred to as M-ANN (M = GM, JL, etc.).

In the following section, simulations are conducted in both PSR and CFD contexts using the optimized global mechanisms and the results are compared with those obtained using the GRI-3.0 mechanism for further evaluation and analysis.

Results and discussion

Performance in PSR simulation

Figure 3 compares the error function value (Err) of the calculated CO mole fraction (X_{CO}) obtained from the optimized global mechanisms to those calculated using GRI-3.0 across different T_{PSR} and f_{O2} conditions. Err, as defined by Hu et al. (Hu et al. 2020) measures the prediction accuracy of the simulated X_{CO}. It is calculated using the following formula:

$$Err = \frac{1}{C}\sum_{i=1}^{C}\left(\left|\frac{\log_{10}\left(X_{CO,i}\right) - \log_{10}\left(X_{CO,i}^{GRI-3.0}\right)}{\log_{10}\left(X_{CO,i}^{GRI-3.0}\right)}\right|\right) \quad (7)$$

where $X_{CO,i}$ is the CO mole fraction of the i-th data point and C is the total number of data points in the datasets. To calculate Err, the dataset is selected based on the time when X_{CO} reaches its peak, $\tau_{CO,max} = a \times 10^d$ sec. Fifteen points are then selected around this time: $1 \times 10^{d-1}$, $2 \times 10^{d-1}$, $4 \times 10^{d-1}$, $6 \times 10^{d-1}$, $8 \times 10^{d-1}$, 1×10^{d}, . . . , $8 \times 10^{d+1}$, and $1 \times 10^{d+1}$ sec.

Moreover, Figure 4 presents the mole fractions of CH_4, O_2, and CO in these cases. For clarity, only the results from the four global mechanisms (GM-ANN, JL-ANN, M5–1-ANN, and M5–2-ANN) with the lowest average error values (Err) are shown, along with those from the GRI-3.0 mechanism.

As shown in Figure 3, the average Err across all global mechanisms shows minimal variation. Moreover, after parameter optimization, the species conversion processes predicted by these global mechanisms are remarkably similar (see Figure 4). The simulated CH_4 decomposition rates and CO peak values align closely with those obtained using the GRI-3.0 mechanism, underscoring the robustness of the ANN-based parameter optimization method.

Furthermore, Figure 3 suggests that Err is more sensitive to T_{PSR} than f_{O2}. Specifically, as T_{PSR} increases, Err rapidly decreases. This trend is also evident in the X_{CO} curves in Figure 4, where the X_{CO} curve from the global mechanisms approaches that of the GRI-3.0 mechanism as T_{PSR} increases. This behavior can be attributed to the suppression of CO to CO_2 conversion at higher T_{PSR}, leading to a broader decline in the X_{CO} curve of the GRI-3.0 mechanism, making it similar to those generated by the global mechanisms. These observations suggest that the global mechanisms are particularly well suited for simulating combustion at high reaction temperatures.

Performance in CFD simulations

Performance in non-premixed flame systems

Figure 5(a) shows the relative errors of the CO concentration (RE_{CO}) for NP-JHC flames, comparing simulations from various global mechanisms against the benchmark GRI-3.0 results at different f_{O2} and T_{coflow}. In Figure 5(b), the relative errors in the temperature distribution (RE_T) are shown for the four global mechanisms with the lowest averaged RE_{CO} (JL-ANN, GM-ANN, M5–4-ANN, and M6-ANN). RE_{CO} and RE_T quantify the relative errors in CO concentration and temperature distributions, respectively, using volume averaging. The calculation process is as follows: (i) identify the regions where $X_{CO}/X_{CO,max} \geq 0.05$ in the GRI-3.0 simulation results, marking these as the combustion reaction zone. (ii) calculate RE_{CO} and RE_T within this zone:

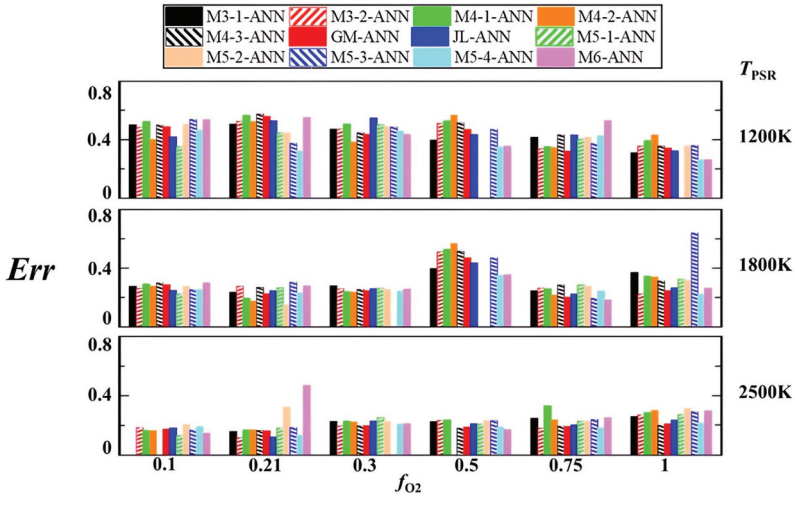

Figure 3. Err of X_{CO} for different ANN-optimized global mechanisms.

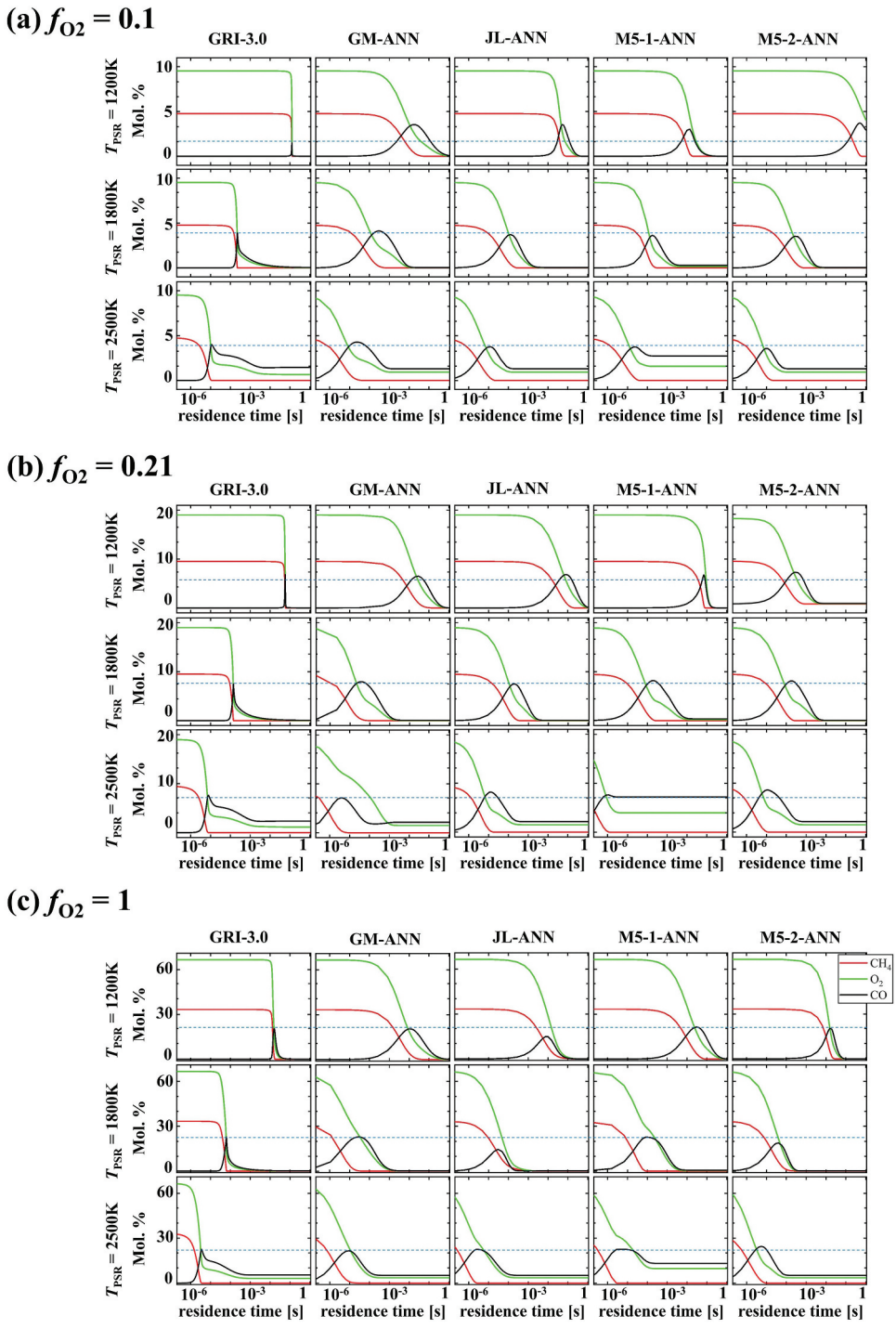

Figure 4. Comparison of CH_4, O_2, and CO concentrations from four global mechanisms (GM-ANN, JL-ANN, M5–1-ANN, and M5–2-ANN) with GRI-3.0 results at Φ = 1.0 and T_{PSR} = 1200, 1800, and 2500 K.

$$RE_M = \frac{\int ARE.dV}{\int dV} \tag{8}$$

$$ARE_M = \left| \frac{M_{GRI-3.0} - M_{Global}}{M_{GRI-3.0}} \right| \tag{9}$$

where M represents a specific physical quantity (e.g., X_{CO} and T).

As shown in Figure 5, GM-ANN exhibits the lowest RE_{CO} = 0.064. Specifically, $RE_{CO,GM\text{-}ANN} < RE_{CO,M6\text{-}ANN} < RE_{CO,JL\text{-}ANN} < RE_{CO,M5\text{-}4\text{-}ANN}$, and $RE_{T,GM\text{-}ANN} < RE_{T,M5\text{-}4\text{-}ANN} < RE_{T,M6\text{-}ANN} < RE_{T,JL\text{-}ANN}$, indicating that the simulation results using the GM mechanism are the closest to those obtained with GRI-3.0. Moreover, RE_{CO} at T_{coflow} = 1800 K and 2500 K are generally lower than that at T_{coflow} = 1200 K, suggesting that global mechanisms perform better in simulating combustion at higher temperatures, consistent with PSR simulations. Additionally, the relatively low RE_T values for GM-ANN indicate more accurate predictions of combustion temperatures. RE_T is generally lower than RE_{CO}, for instance, averaged RE_T

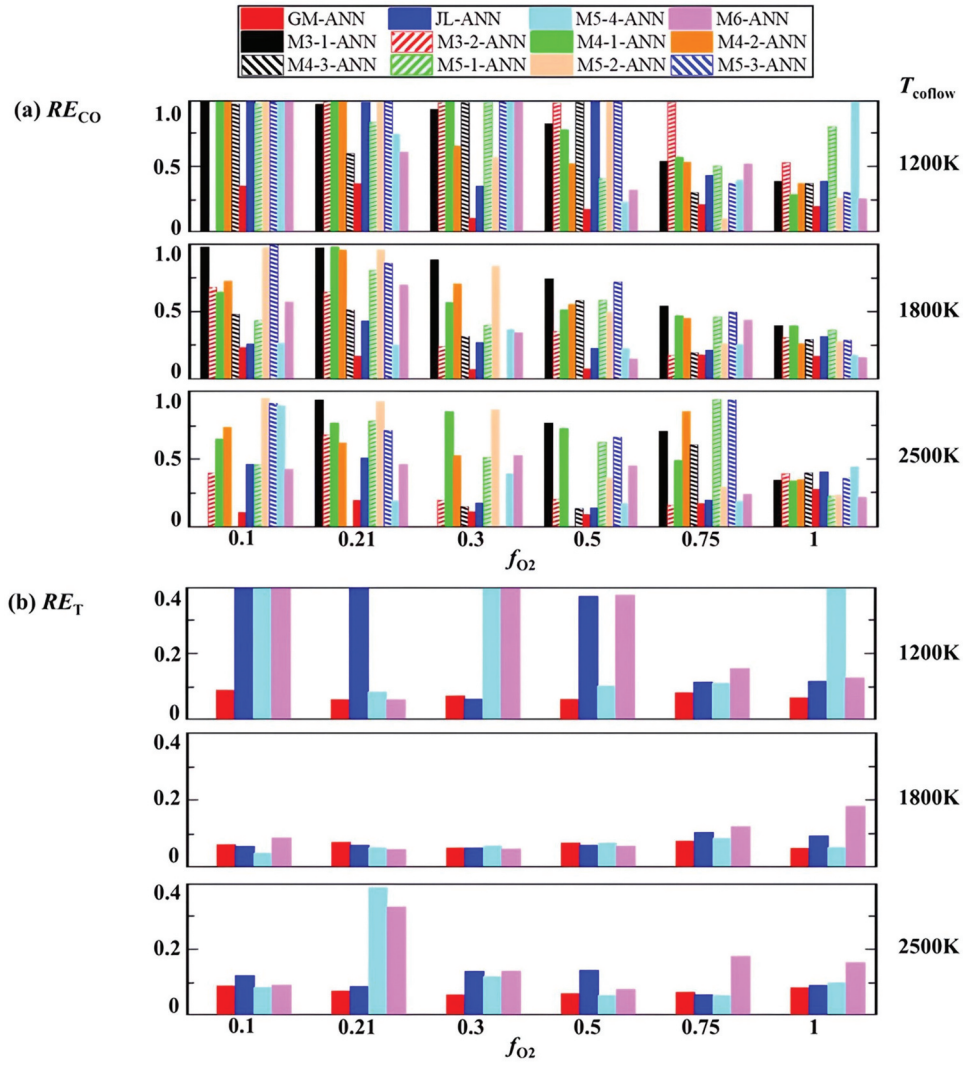

Figure 5. (a) RE_{CO} and (b) RE_T for different global mechanisms in NP-JHC simulations at different f_{O2} and T_{coflow}.

($RE_{T,averaged}$) = 0.066 is smaller than averaged RE_{CO} ($RE_{CO,averaged}$) = 0.185 in NP-JHC simulations. This may be due to the lower CO concentration in the reaction zone, resulting in larger relative errors.

Figure 6 illustrates contours of CO concentration (X_{CO}) in NP-JHC flames obtained from four mechanisms with the lowest $RE_{CO,averaged}$ (GM-ANN, JL-ANN, M5–4-ANN, and M6-ANN) and the detailed GRI-3.0 mechanism. Results from the M3–2-ANN mechanism are demonstrated to highlight the significance of reaction R5. The GM-ANN mechanism closely matches the X_{CO} distribution from the GRI-3.0 simulations, while other global mechanisms show significant deviations, especially on the fuel-rich side where X_{CO} is generally overestimated. These discrepancies become more pronounced as f_{O2} decreases. At f_{O2} = 1, however, the performance of these mechanisms is comparable.

These significant discrepancies in predicting the X_{CO} distribution can be largely attributed to R2 ($CH_4 + H_2O \rightarrow CO + 3\,H_2$), which enhances CO production on the fuel-rich side. Moreover, the reversible reaction R4 ($CO + H_2O \leftrightarrow CO_2 + H_2$) also contributes to CO formation under these conditions, as supported by previous studies (Si et al. 2020). Therefore, R2 is inadequate for accurately modeling CH_4 decomposition in non-premixed conditions.

Furthermore, M3–2-ANN underestimates X_{CO}, which may stem from the lack of competition between reactions R5 ($CO + 0.5\,O_2 \leftrightarrow CO_2$) and R6 ($H_2 + 0.5\,O_2 \leftrightarrow H_2O$) for O_2. This imbalance leads to an overproduction of H_2O and subsequently driving R4 to consume more CO. These results highlight the importance of including R5 and excluding R2 for accurate X_{CO} simulation under NP-JHC conditions.

Figure 7 presents the RE_{CO} and RE_T values for various global mechanisms within the NPF flame system. Stable flames could not be achieved at a wall temperature (T_{wall}) of 1200 K with $f_{O2} \leq 0.5$. Among the mechanisms evaluated, GM-ANN consistently shows the lowest RE_{CO} and RE_T (0.050 and 0.027), as observed in NP-JHC flames. As f_{O2} and T_{wall} increase, a distinct decrease in RE_{CO} is observed for GM-ANN, primarily because higher f_{O2} and T_{wall} enhance the combustion intensity and temperature. Additionally, elevated f_{O2} and T_{wall} reduce the dilution effect of N_2, resulting in higher X_{CO} and T, which increases the denominator in the calculations for RE_T and RE_{CO}.

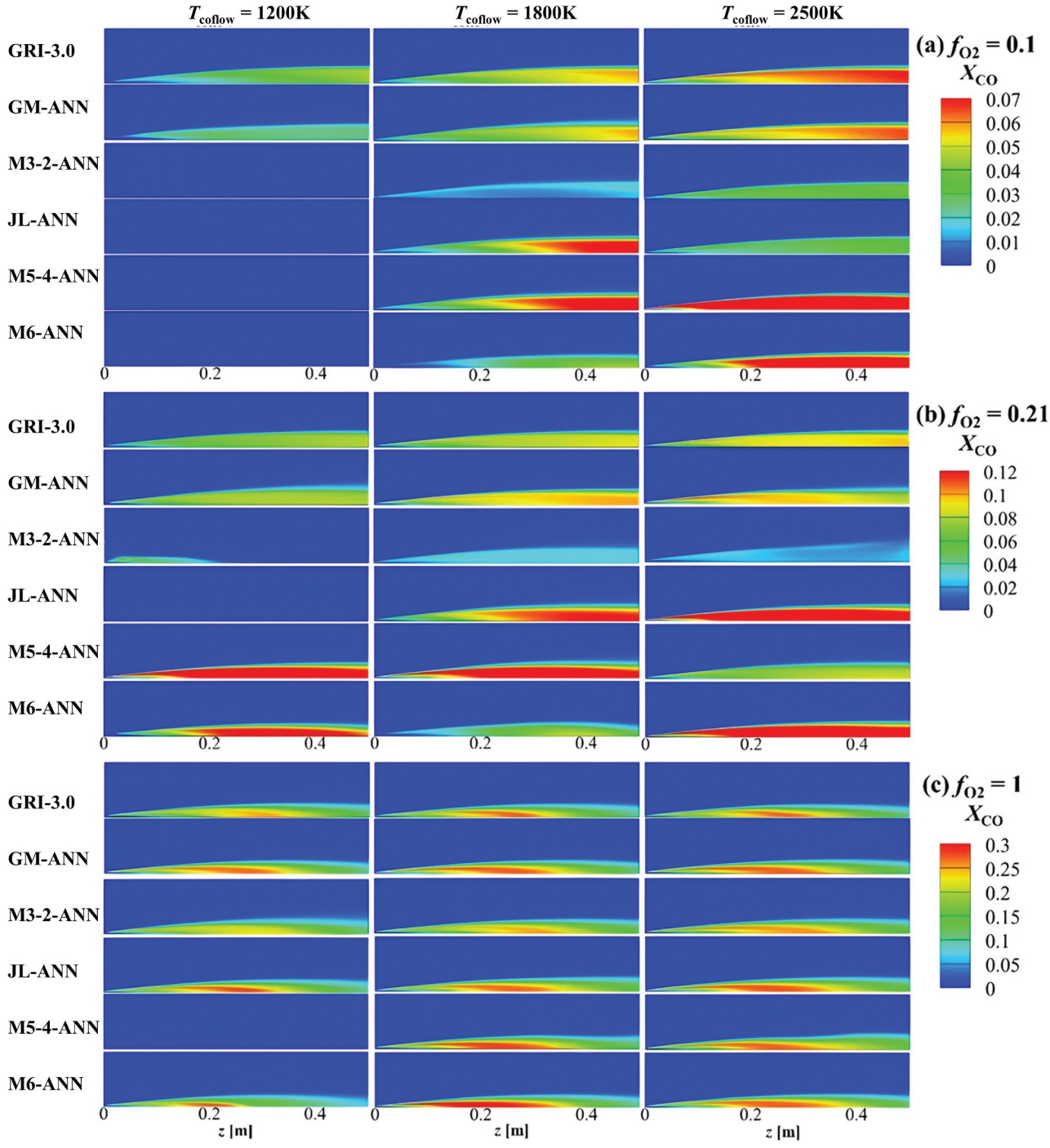

Figure 6. Contour distributions of X_{CO} for different global mechanisms and GRI-3.0 in NP-JHC simulations under different f_{O2} and T_{coflow}.

Figure 8 compares the X_{CO} distributions simulated using GRI-3.0 with those from the four mechanisms exhibiting the lowest $RE_{CO,averaged}$ (GM-ANN, JL-ANN, M4–3-ANN, and M5–4-ANN). GM-ANN simulations align most closely with the GRI-3.0 results. In contrast, the other global mechanisms tend to overestimate X_{CO}, primarily due to the inclusion of reaction R2.

In summary, for non-premixed combustion systems, GM-ANN generally exhibits the lowest $RE_{CO,averaged}$ and $RE_{T,averaged}$ (0.179 and 0.137), indicating that its X_{CO} and T distributions are most closely aligned with those of the detailed GRI-3.0 mechanism. Furthermore, a systematic comparative analysis of the averaged RE_M ($RE_{M,averaged}$) for all global mechanisms under non-premixed conditions is provided in Supplementary Material.

Performance in premixed flame systems

Figure 9 presents the calculated RE_{CO} and RE_T for the global mechanisms within P-JHC system under different f_{O2} and T_{coflow}. At T_{coflow} = 1800 and 2500 K, the JL-ANN mechanism consistently exhibits much lower RE_{CO} and RE_T values than

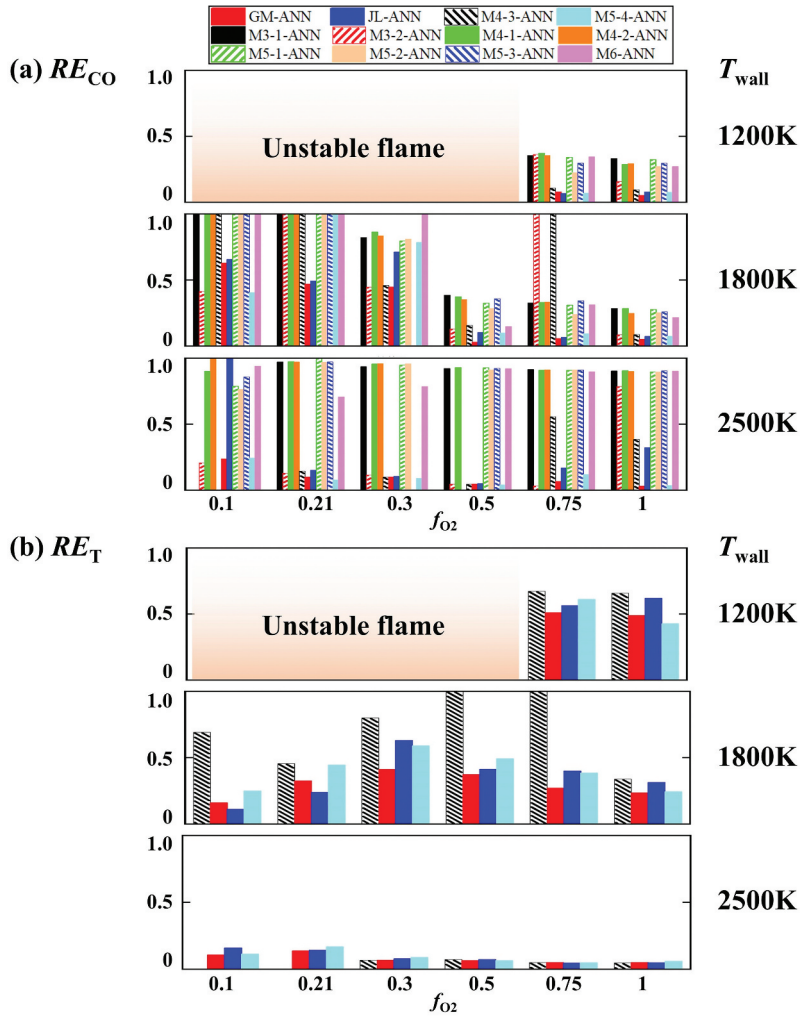

Figure 7. (a) RE_{CO} and (b) RE_T for different ANN-optimized global mechanisms in NPF simulations at various f_{O2} and T_{wall}.

the other global mechanisms. At $T_{coflow} = 1200$ K, stable premixed flame could not be achieved by these mechanisms.

Figure 10 compares the X_{CO} distribution in P-JHC simulations from the four most accurate global mechanisms (JL-ANN, M3–2-ANN, GM-ANN, and M5–4-ANN) with that of the GRI-3.0 mechanism. The JL-ANN simulations closely match the GRI-3.0 results. In contrast, the GM-ANN mechanism underestimates the CO concentration at $T_{coflow} = 1800$ K, whereas it overestimates CO concentration at $T_{coflow} = 2500$ K. This discrepancy can be attributed to the dual CO consumption reactions in GM-ANN, R4 and R5. At $T_{coflow} = 1800$ K, these reactions lead to an overestimation of CO consumption. Conversely, at 2500 K, the high temperature shifts the equilibrium of R5 toward CO production, resulting in an overestimation of CO concentration. This conclusion is further supported by comparing GM-ANN with M3–2-ANN, where R5 is not included.

Compared to JL-ANN, the M3–2-ANN mechanism overestimates X_{CO} due to the lack of reaction R2. The JL-ANN mechanism improves $CH_4 \rightarrow H_2O$ conversion through R2, which enhances CO consumption via R6. This highlights the importance of R2 in CO conversion under premixed combustion conditions. Additionally, the presence of multiple R3 reactions in the M5–4-ANN mechanism leads to an overestimation of CO production in the simulations. Consequently, for simulating premixed jet flames, the JL-ANN mechanism is most effective in accurately describing combustion and CO conversion processes.

The reactant mixing mode significantly affects the performance of global mechanisms, whereas f_{O2} and T_{coflow} have minimal impact. In non-premixed combustion systems, where fuel and oxidizer are not mixed before combustion reactions, the global reaction rates of CH_4 are slower, thus the production rates of CO and H_2 are very low ($CH_4 + 0.5O_2 \rightarrow CO + 2H_2$) on the fuel-rich side. Moreover, the reverse reaction R4 can generate excessive CO, preventing its consumption by R5. Conversely, under premixed conditions, where the fuel and oxidizer are initially mixed, the reaction rate of CH_4 is faster, resulting in higher global combustion rates.

Figure 11 compares the RE_{CO} and RE_T values of various global mechanisms in PF simulations. At $T_{wall} = 1200$ K, both RE_{CO} and RE_T are notably higher than those at $T_{wall} = 1800$ K and 2500 K, with RE_{CO} generally exceeding 0.5. In the PF

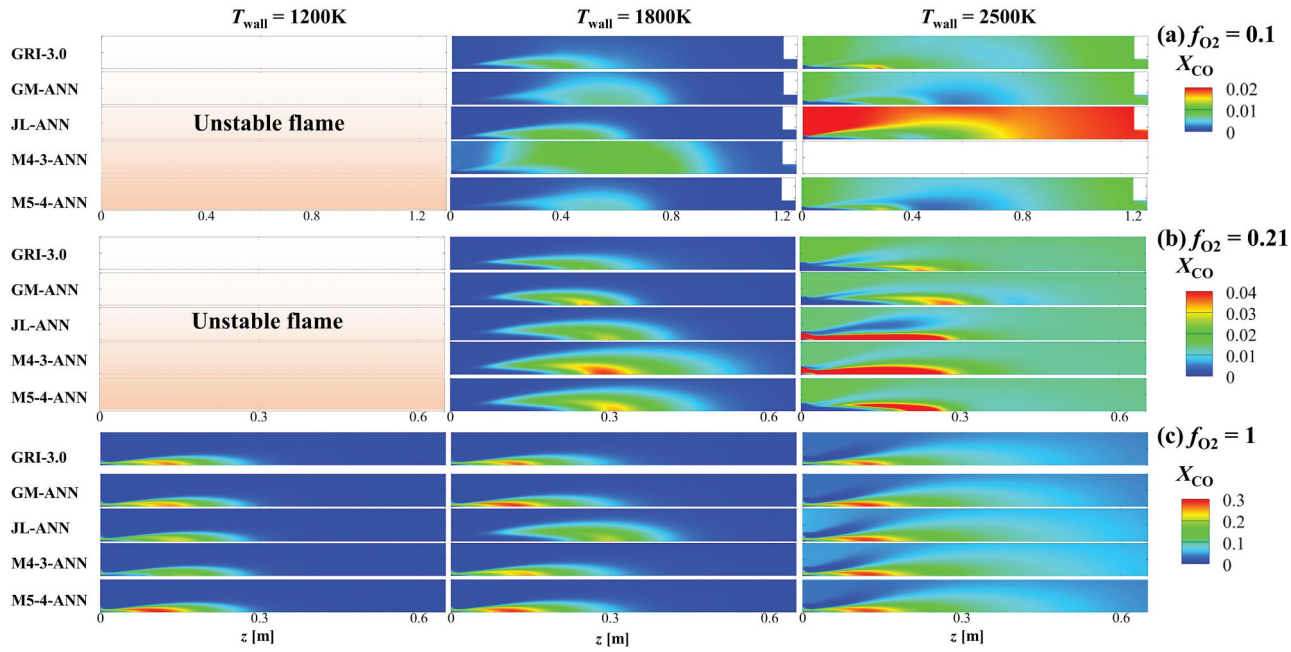

Figure 8. Contour distributions of X_{CO} for different global mechanisms and GRI-3.0 in NPF simulations at various f_{O2} and T_{wall}.

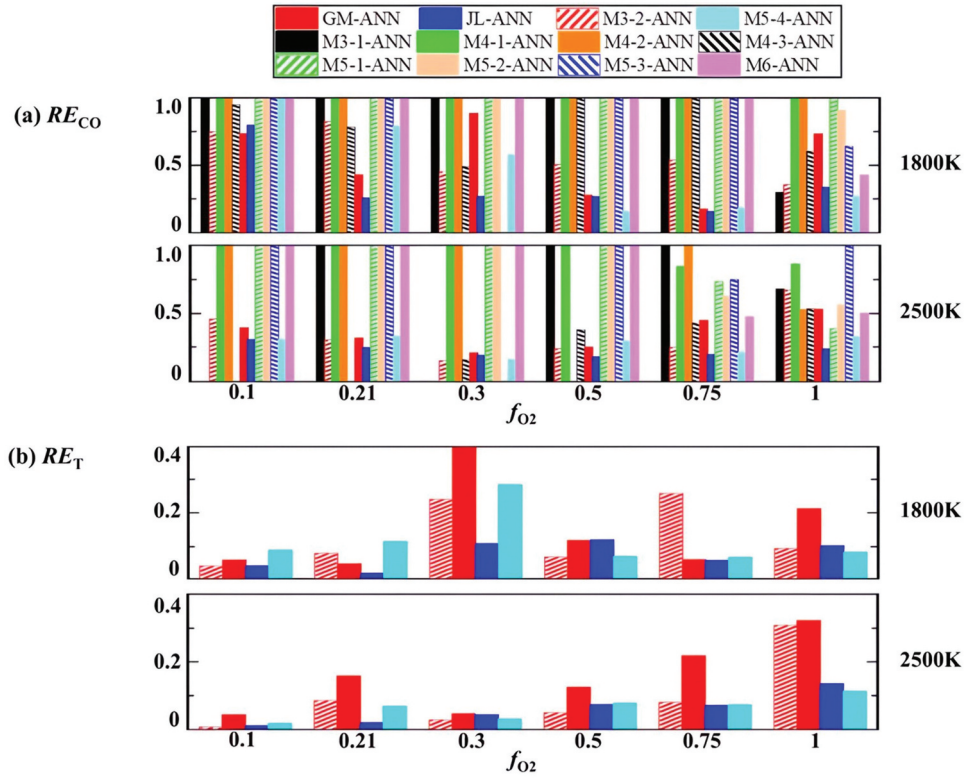

Figure 9. (a) RE_{CO} and (b) RE_T for different global mechanisms in P-JHC simulations at various f_{O2} and T_{coflow}.

simulation, JL-ANN outperforms the other mechanisms, particularly at $T_{wall} = 1800$ and 2500 K. Moreover, as T_{wall} increases, both RE_{CO} and RE_T show a decreasing trend, consistent with observations in the NPF cases.

Figure 12 shows the X_{CO} distribution in PF simulations of four global mechanisms with the lowest$RE_{CO,averaged}$ (JL-ANN, M3–2-ANN, GM-ANN, and M5–3-ANN) and that of GRI-3.0. Among these, the X_{CO} levels simulated using JL-ANN most closely match those of GRI-3.0. However, M3–2-ANN and

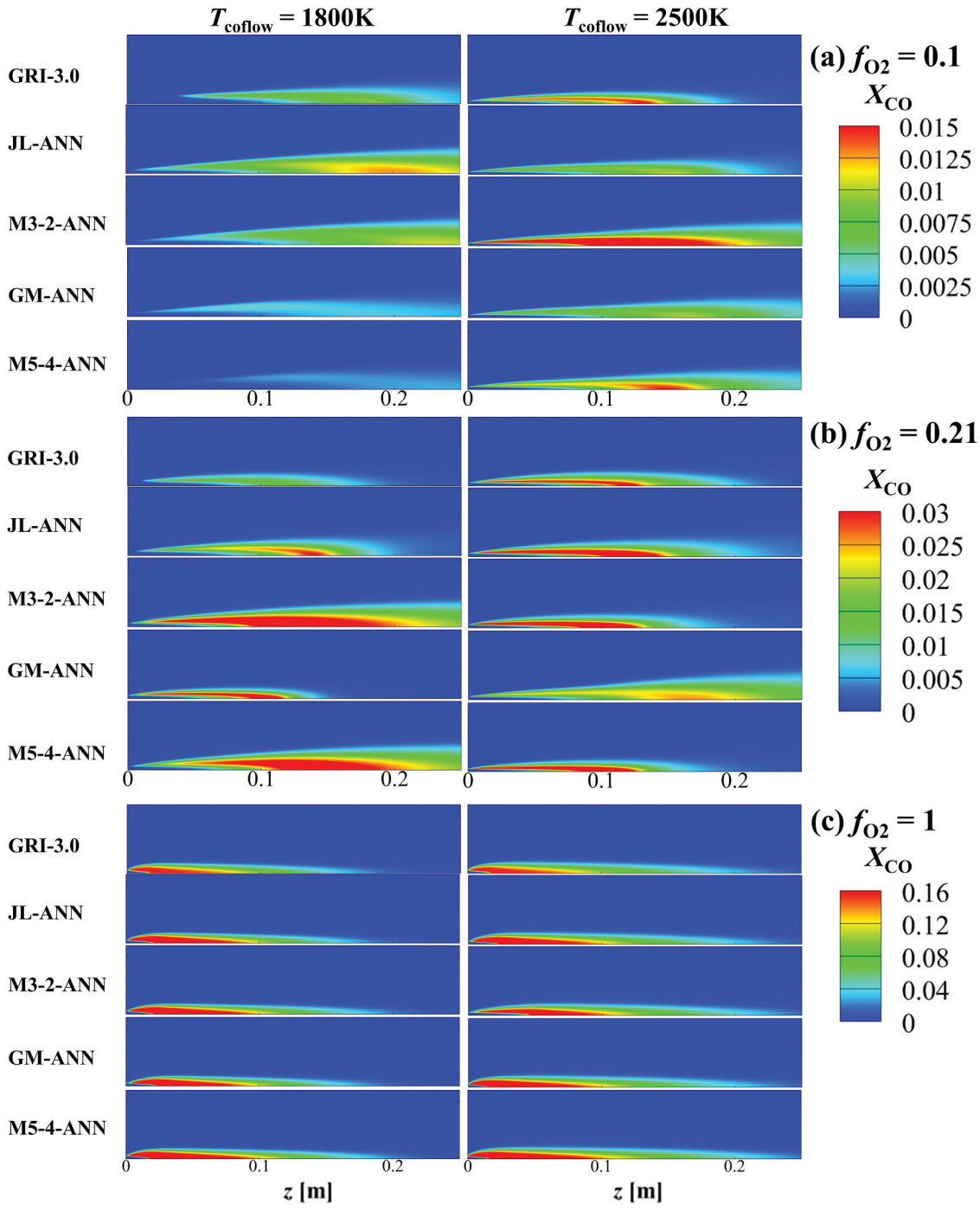

Figure 10. Contour distributions of X_{CO} for different global mechanisms and GRI-3.0 in P-JHC simulations under different f_{O2} and T_{coflow}.

GM-ANN generally overestimate X_{CO} in most cases, except at $f_{O2} = 0.1$ with $T_{wall} = 1800$ K and at $f_{O2} = 1$ with $T_{wall} = 1200$ K. This overestimation is likely due to the absence of R2, which results in a lower H_2O production rate and, consequently, a reduced CO-CO_2 conversion rate via R4. Additionally, the presence of R3 in M5–3-ANN leads to an overestimation of the peak X_{CO} value. In summary, the JL-ANN provides the most accurate simulations ($RE_{CO,averaged} = 0.354$, $RE_{T,averaged} = 0.048$) for premixed combustion, closely aligning with the GRI-3.0 results. A detailed quantitative comparison of the $RE_{M,averaged}$ for all global mechanisms under premixed conditions is provided in Supplementary Material.

Conclusions

Global mechanisms play a critical role in improving the computational efficiency of methane combustion simulations. However, existing studies on global mechanisms have primarily focused on individual or limited operating conditions, without providing a comprehensive evaluation across varying

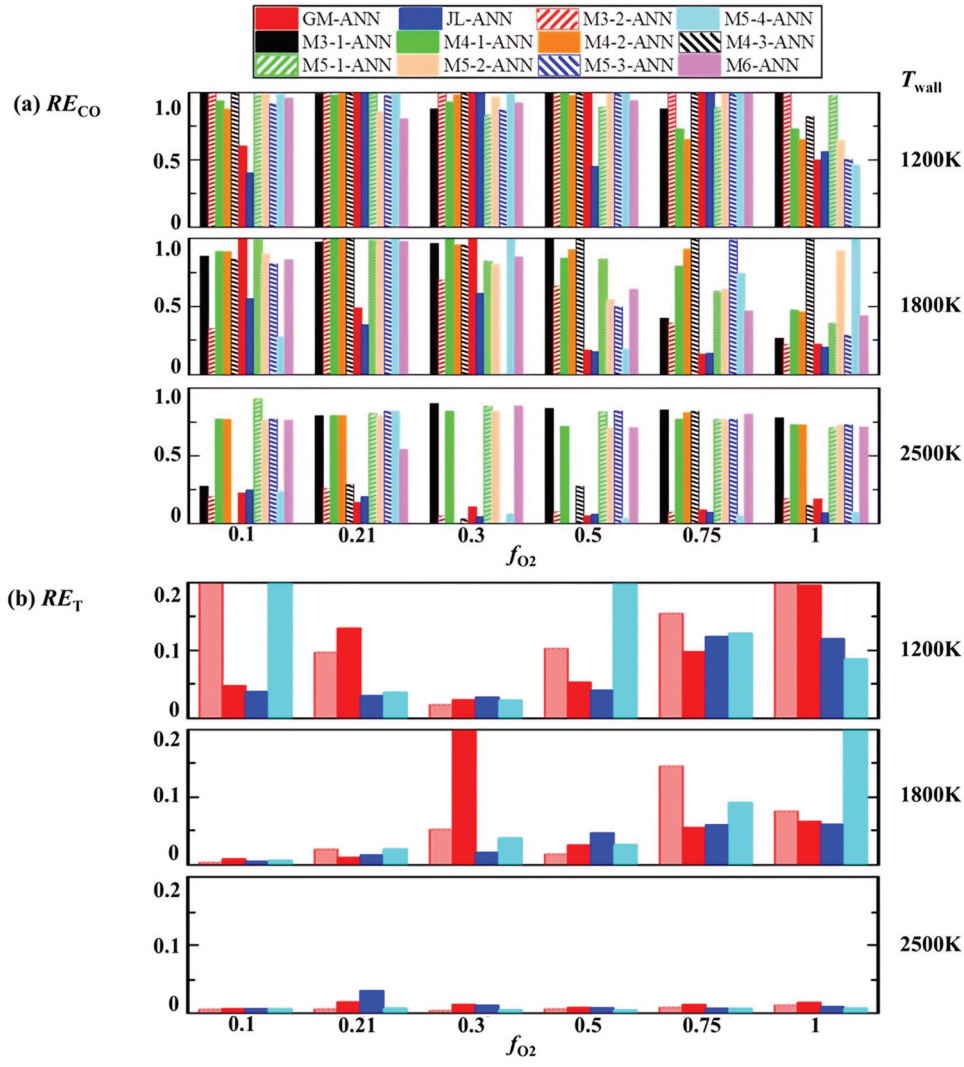

Figure 11. (a) RE_{CO} and (b) RE_T for different global mechanisms in PF simulations at different f_{O2} and T_{wall}.

combustion environments. Therefore, the predictive reliability of these mechanisms under different reaction scenarios remains unclear. To address this, the present study conducts systematic evaluation of existing global mechanisms for methane combustion by comparing their predictions of temperature and CO distribution against those obtained using the detailed mechanism GRI-Mech 3.0. The evaluation is performed across a wide range of operating conditions, including temperatures from 1200 K to 2500 K, oxygen mole fractions from 0.1 to 1.0, and different mixing regimes (premixed and non-premixed), within both jet flame and in-furnace configurations. The main findings of this research are summarized as follows:

(1) In PSR simulations, the global mechanisms exhibit good applicability at high T_{PSR}. In CFD simulations of non-premixed combustion, increasing f_{O2} and T_{wall}/T_{coflow} leads to a decrease in RE_{CO} for GM-ANN, primarily because higher f_{O2} and T_{wall}/T_{coflow} enhance the combustion intensity and temperature. Additionally, elevated f_{O2} and T_{wall}/T_{coflow} reduce the dilution effect of N_2, resulting in higher X_{CO} and T, which increases the denominator in the calculations for RE_T and RE_{CO}. In PF cases, a similar influence is observed with T_{wall} variation alone.

(2) In CFD simulations of non-premixed combustion, the GM-ANN mechanism outperforms other global mechanisms, closely aligning with GRI-3.0 in terms of X_{CO} ($RE_{CO,averaged} = 0.179$) and temperature distributions ($RE_{T,averaged} = 0.137$). Comparative analysis reveals that reaction R2 ($CH_4 + H_2O \rightarrow CO + 3\,H_2$) significantly affects X_{CO} distribution on the fuel-rich side. Moreover, the competitive interaction between R5 ($CO + 0.5O_2 \leftrightarrow CO_2$) and R6 ($H_2 + 0.5O_2 \leftrightarrow H_2O$) mitigates the overestimation of H_2O production, leading to more accurate X_{CO} predictions.

(3) In CFD simulations of premixed combustion, the JL-ANN mechanism provides the most accurate X_{CO} ($RE_{CO,averaged} = 0.354$) and temperature distributions ($RE_{T,averaged} = 0.048$) when compared to GRI-3.0. Under these conditions, R2 plays a pivotal role in converting CO intermediate species. Conversely, the

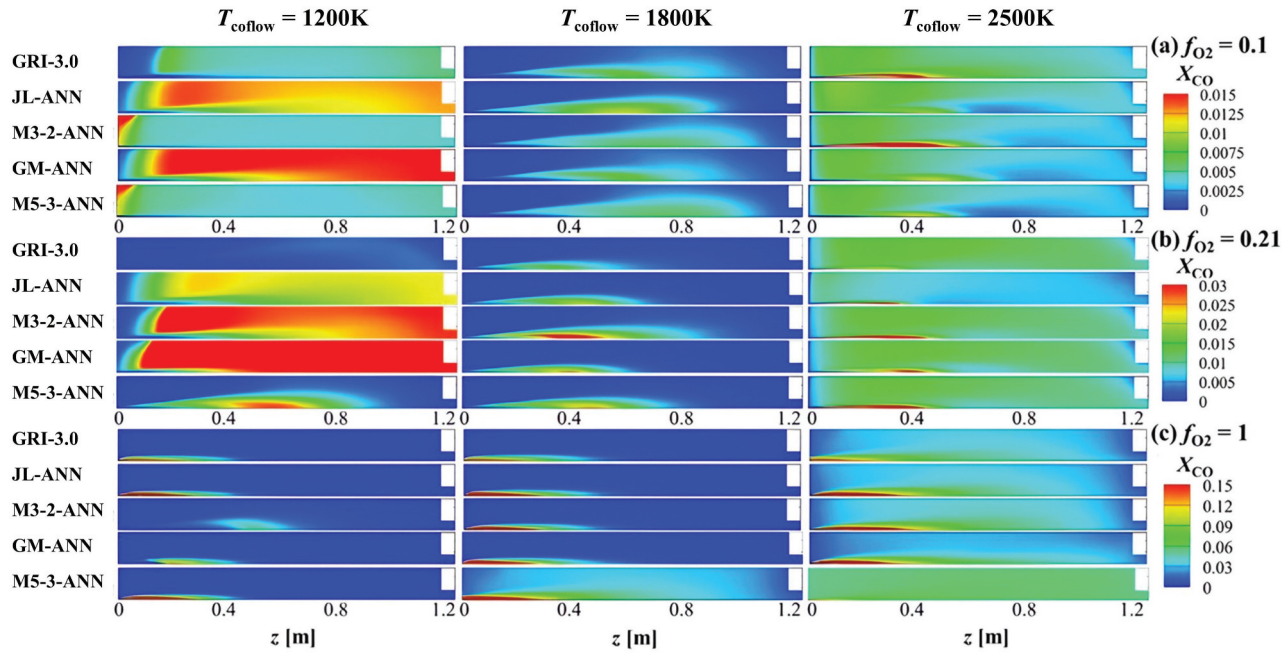

Figure 12. Contour distributions of X_{CO} for different global mechanisms and GRI-3.0 in PF simulations under different f_{O2} and T_{wall}.

inclusion of R5 in GM-ANN leads to incorrect CO conversion rates under premixed conditions.

(4) Our analysis of both premixed and non-premixed combustion highlights the critical importance of the reactant mixing mode in selecting the optimal global mechanism. Furthermore, discrepancies between the performances of global mechanisms in CFD simulations versus PSR results suggest a further validation when the reaction parameters are optimized.

Acknowledgments

Shuang Li and **Xiangtao Liu** contributed equally to this work. **Shuang Li & Xiangtao Liu**: Writing – review & editing, Writing – original draft, Visualization, Validation, Software, Methodology, Investigation, Formal analysis, Data curation, Conceptualization. **Jicang Si**: Writing – review & editing, Supervision, Resources, Conceptualization, Funding acquisition. **Guochang Wang**: Writing – review & editing, Investigation, Funding acquisition. **Yuanye Guo**: Writing – review & editing. **Mengwei Wu**: Writing – review & editing. **Enguang Xu**: Writing – review & editing. **Minyi Xu**: Writing – review & editing, Supervision, Resources. **Jianchun Mi**: Writing – review & editing, Supervision, Resources.

Author contributions

CRediT: **Shuang Li:** Conceptualization, Data curation, Formal analysis, Investigation, Methodology, Software, Validation, Visualization, Writing – original draft, Writing – review & editing; **Xiangtao Liu:** Conceptualization, Data curation, Formal analysis, Investigation, Methodology, Software, Validation, Visualization, Writing – original draft, Writing – review & editing; **Jicang Si:** Conceptualization, Funding acquisition, Resources, Supervision, Writing – review & editing; **Guochang Wang:** Funding acquisition, Investigation, Writing – review & editing; **Yuanye Guo:** Writing – review & editing; **Mengwei Wu:** Writing – review & editing; **Enguang Xu:** Writing – review & editing; **Minyi Xu:** Resources, Supervision, Writing – review & editing; **Jianchun Mi:** Resources, Supervision, Writing – review & editing.

Disclosure statement

No potential conflict of interest was reported by the author(s).

Funding

The authors greatly acknowledge the support of the National Natural Science Foundation of China (No. 52206145), the Basic Research Funds of Liaoning Universities (No. LJ212410151008), and high-performance computing platform of Peking University.

Nomenclature

Symbols

A	pre-exponential factor ((cm3/mol)n-1/sec), where n is the reaction order
b	temperature exponent
E_a	activate energy (Kcal/mol)
Err	error function value
f_m	inlet mole fraction for species m
k	chemical reaction rate constant
r	radial coordinate (mm)
R	gas constant (m3·atm/K·kmol)
RE_{CO}	relative error of CO mole fraction distribution
$RE_{CO,averaged}$	averaged relative error of CO mole fraction distribution
RE_T	relative error of temperature distribution
$RE_{T,averaged}$	averaged relative error of temperature distribution
T	temperature (K)
T_{coflow}	coflow temperature (K)
T_{wall}	wall temperature (K)
T_{PSR}	temperature of perfectly stirred reactor (K)
z	axial coordinate (mm)

X_m	mole fraction for species m
Greek letters	
Φ	equivalence ratio

Abbreviations

GRI-3.0	GRI-Mech 3.0
ANN	Artificial neural network\
ARE	Absolute value of the relative error
GM	global mechanism for MILD combustion proposed in the present study
M-ANN	mechanism M with ANN-optimized reaction parameters
NPF	non-premixed furnace
NP-JHC	Jet-in-Hot-Coflow under non-premixed condition
JHC	Jet-in-Hot-Coflow
JL	Jones and Lindestedt's mechanism
MILD	Moderate or intense low-oxygen dilution
PF	premixed straight-flow furnace
P-JHC	Jet-in-Hot-Coflow under premixed condition
PSR	perfectly stirred reactor
RANS	Reynolds-averaged Navier-Stokes
WD	Westbrook and Dryer's mechanism
WSGGM	Weight Sum of Gray Gases Model

References

Abou-Taouk, A., S. Sadasivuni, D. Lörstad, and L. E. Eriksson. 2013. Evaluation of global mechanisms for LES analysis of SGT-100 DLE combustion system. In ASME turbo expo 2013: Turbine technical conference and expositio, ed. B. Winkelmann, V01BT04A03. USA: San Antonio.

Amini, A., A. Anaraki Haji Bagheri, M. H. Sedaghat, and M. R. Rahimpour. 2023. CFD simulation of an industrial steam methane reformer: Effect of burner fuel distribution on hydrogen production. *Fuel* 352:129008. doi: 10.1016/j.fuel.2023.129008.

Andersen, J., C. L. Rasmussen, T. Giselsson, and P. Glarborg. 2009. Global combustion mechanisms for use in CFD modeling under oxy-fuel conditions. *Energy Fuels* 23 (3):1379–89. doi: 10.1021/ef8003619.

ANSYS® Fluent. 2022. *(Version 22.1.0, 2022R1)*. Canonsburg, PA: ANSYS, Inc.

ANSYS Fluent. 2017. *(Version 15180, 18.0)*. San Diego: ANSYS, Inc.

Christo, F. C., and B. B. Dally. 2005. Modeling turbulent reacting jets issuing into a hot and diluted coflow. *Combustion and Flame* 142 (1–-2):117–29. doi: 10.1016/j.combustflame.2005.03.002.

Chui, E. H., and G. D. Raithby. 1993. Computation of radiant heat transfer on a nonorthogonal mesh using the finite-volume method. *Numer Heat Tr b-Fund* 23 (3):269–88. doi: 10.1080/10407799308914901.

Dally, B., A. Karpetis, and R. Barlow. 2002. Structure of turbulent non-premixed jet flames in a diluted hot coflow. *Proceedings of the Combustion Institute International Symposium on Combustion* 29 (1):1147–54. doi: 10.1016/S1540-7489(02)80145-6.

Di, H., Y. Yusong, K. Yucheng, and W. Chaojun. 2022. Analysis of EDC constants for predictions of methane MILD combustion. *Fuel* 324:124542. doi: 10.1016/j.fuel.2022.124542.

Doan, N. A. K., and N. Swaminathan. 2019. Autoignition and flame propagation in non-premixed MILD combustion. *Combustion and Flame* 201:234–43. doi: 10.1016/j.combustflame.2018.12.025.

Doan, N. A. K., N. Swaminathan, and Y. Minamoto. 2018. DNS of MILD combustion with mixture fraction variations. *Combustion and Flame* 189:173–89. doi: 10.1016/j.combustflame.2017.10.030.

Dunn-Rankin, D. 2011. Lean combustion: Technology and control. *Nano Letters* 11 (4):1831–37. doi: 10.1021/nl2006164.

Farokhi, M., and M. Birouk. 2020. Assessment of Fractal/Wrinkling theories for describing turbulent reacting fine structures under MILD combustion regimes. *Combustion Science and Technology* 193 (10):1798–825. doi: 10.1080/00102202.2020.1715963.

Frassoldati, A., A. Cuoci, T. Faravelli, E. L. I. S. E. O. Ranzi, C. Candusso, and D. Tolazzi. 2008. Simplified kinetic schemes for oxy-fuel combustion. *1st International conference on sustainable fossil fuels for future energy*, Rome, Italy.

Frenklach M.H. Wang, C. L. Yu, M. Goldenberg, C. T. Bowman, R. K. Hanson, D. F. Davidson, E. J. Chang, G. P. Smith, D. M. Golden,W. C Gardiner, and V. Lissianski. 1995. *GRI-Mech 1.2*. http://www.me.berkeley.edu/gri_mech/

Fursenko, R. V., V. V. Gubernov, V. A. Kosyakov, A. A. Shupik, and B. Kichatov. 2020. Combustion of lean methane–air flames in mesoscale reactor with opposite gas flows. *Combustion Science and Technology* 194 (9):1872–94. doi: 10.1080/00102202.2020.1842381.

Galletti, C., A. Parente, and L. Tognotti. 2007. Numerical and experimental investigation of a mild combustion burner. *Combustion and Flame* 151 (4):649–64. doi: 10.1016/j.combustflame.2007.07.016.

Harvazinski, M. E., D. G. Talley, and V. Sankaran. 2016. Application of detailed chemical kinetics to combustion instability modeling. 54th AIAA Aerospace Sciences Meeting, San Diego, CA, USA.

Hu, F., P. Li, J. Guo, Z. Liu, L. Wang, J. Mi, B. Dally, and C. Zheng. 2018. Global reaction mechanisms for MILD oxy-combustion of methane. *Energy* 147:839–57. doi: 10.1016/j.energy.2018.01.089.

Hu, F., P. Li, K. Wang, W. Li, J. Guo, L. Liu, and Z. Liu. 2020. EvaluatiEvaluatiOn, development, and application of a new skeletal mechanism for fuel-NO formation under air and oxy-fuel combustion. *Fuel Processing Technology* 199:106256. doi: 10.1016/j.fuproc.2019.106256.

Jones, W. P., and R. P. Lindstedt. 1988. Global reaction schemes for hydrocarbon combustion. *Combustion and Flame* 73 (3):233–49. doi: 10.1016/0010-2180(88)90021-1.

Kim, J. P., U. Schnell, and G. Scheffknecht. 2008. Comparison of different global reaction mechanisms for MILD combustion of natural gas. *Combustion Science and Technology* 180 (4):565–92. doi: 10.1080/00102200701838735.

Kiran, D., Y. Minamoto, K. Osawa, M. Shimura, and M. Tanahashi. 2023. A direct numerical simulation study for flame structure and propagation characteristics of multi-jet flames. *Combustion Science and Technology* 196 (18):5064–88. doi: 10.1080/00102202.2023.2249220.

Kuang, Y., B. He, C. Wang, W. Tong, and D. He. 2022. Numerical research for MILD burners with different configurations. *Combustion Science and Technology* 196 (3):421–38. doi: 10.1080/00102202.2022.2081919.

Lamioni, R., P. E. Lapenna, L. Berger, K. Kleinheinz, A. Attili, H. Pitsch, and F. Creta. 2020. Pressure-induced hydrodynamic instability in premixed methane-air slot flames. *Combustion Science and Technology* 192 (11):1998–2009. doi: 10.1080/00102202.2020.1768081.

Li, X., Z. Peng, Y. Pei, T. Ajmal, K. J. Rana, A. Aitouche, and R. Mobasheri. 2021. Oxy-fuel combustion for carbon capture and storage in internal combustion engines–A review. *International Journal of Energy Research* 46 (2):505–22. doi: 10.1002/er.7199.

Li, Z., Y. Zhang, and H. Zhang. 2024. Kinetics modeling of NOx emission of oxygen-enriched and rich-lean-staged ammonia combustion under gas turbine conditions. *Fuel* 355:129509. doi: 10.1016/j.fuel.2023.129509.

Liu, Y., J. Liu, Q. Lyu, J. Zhu, F. Pan, and X. Zhang. 2022. Comparison of detailed nitrogen-containing mechanisms in preheating combustion technology under O2/CO2 atmosphere. *Combustion Science and Technology* 196 (3):321–35. doi: 10.1080/00102202.2022.2077103.

Magnussen, B. F. 1981. On the structure of turbulence and a generalized eddy dissipation concept for chemical reaction in turbulent flow. *19th aerospace sciences meeting*, St. Louis, MO, U.S.A., vol. 1, 42, January 12–15.

Manzoor, M. U., X. Dou, M. Yosri, M. Talei, and Y. Yang. 2024. Capturing different modes of hydrogen combustion in a spark-ignition engine using numerical simulations. *Fuel* 375:132343. doi: 10.1016/j.fuel.2024.132343.

Marinov, N. M., and C. K. Westbrook. 1996. Detailed and global chemical kinetics model for hydrogen. *Transport Phenomena in Combustion* 1 (80):118–29.

MATLAB (Version 9.14.0, R). 2023a. *The MathWorks*. Natick, MA: Inc.

Meredith, K., and D. Black. 2006. Automated global mechanism generation for use in CFD simulations. *44th AIAA Aerospace Sciences Meeting and Exhibit*, Reno, Nevada, vol. 1, 1168. 9-12 January.

Minamoto, Y., and N. Swaminathan. 2014. Scalar gradient behaviour in MILD combustion. *Combustion and Flame* 161 (4):1063–75. doi: 10.1016/j.combustflame.2013.10.005.

Normann, F., A. O. Wismer, C. R. Müller, and H. Leion. 2019. Oxidation of ammonia by iron, manganese and nickel oxides – implications on NOx formation in chemical-looping combustion. *Fuel* 240:57–63. doi: 10.1016/j.fuel.2018.11.121.

Pope, S. B. 1978. An explanation of the turbulent round-jet/plane-jet anomaly. *AIAA Journal* 16 (3):279–81. doi: 10.2514/3.7521.

Putra, B. A., and I. S. Ertesvåg. 2023. Investigations of the extended eddy dissipation concept formulation for weakly turbulent and slow chemistry flames. *Fuel* 352:129013. doi: 10.1016/j.fuel.2023.129013.

Rodrigues, L. G. P., I. M. Machado, A. Ziemniczak, F. M. Pereira, P. R. Pagot, and F. H. R. França. 2019. Comparisons between numerical simulations and experimental measurements of radiative heat flux for a series of CH4/N2 diluted laminar non-premixed flames. *Combustion Science and Technology* 193 (1):1–22. doi: 10.1080/00102202.2019.1646733.

Sarr, J. A. R., C. P. T. Groth, and J. C. T. Hu. 2019. A maximum entropy-inspired interpolative closure for the prediction of radiative heat transfer in laminar Co-flow diffusion flames. *Combustion Science and Technology* 194 (1):45–79. doi: 10.1080/00102202.2019.1678376.

Shu, Z., F. Wang, C. Dai, J. Si, B. Wang, and J. Mi. 2020. Characteristics of nitric-oxide emissions from traditional flame and MILD combustion operating in a laboratory-scale furnace. *Journal of Thermal Science* 29 (4):868–83. doi: 10.1007/s11630-020-1235-0.

Si, J., G. Wang, P. Li, and J. Mi. 2020. Optimization of the global reaction mechanism for MILD combustion of methane using artificial neural network. *Energy and Fuels* 34 (3):3805–15. doi: 10.1021/acs.energyfuels.9b04413.

Si, J., G. Wang, X. Liu, M. Wu, and J. Mi. 2021. A New global mechanism for MILD combustion using artificial-neural-network-based optimization. *Energy Fuels* 35 (18):14941–53. doi: 10.1021/acs.energyfuels.1c01820.

Si, J., G. Wang, Z. Shu, X. Liu, M. Wu, R. Zhu, and J. Mi. 2021. Experimental and numerical study on moderate or intense low-oxygen dilution oxy-combustion of methane in a laboratory-scale furnace under N2, CO2, and H2O dilutions. *Energy Fuels* 35 (15):12403–15. doi: 10.1021/acs.energyfuels.1c01590.

Smith, G. P., , D. M. Golden, , M. Frenklach, , N. W. Moriarty, , B. Eiteneer, , M. Goldenberg, , C. T. Bowman, , R. K. Hanson, , S. Song, , J. W. C. Gardiner,V. V Lissianski, and Z. Qin. 1999. *GRI-Mech 3.0*. http://www.me.berkley.edu/gri_mech/

Smooke, M. D. 1991. *Reduced kinetic mechanisms and asymptotic approximations for methane-air flames: a topical volume*. Berlin: Springer-Verlag.

Tu, Y., W. Yang, and H. Liu. 2017. A refined global reaction mechanism for gently preheated MILD combustion of methane. *Energy Fuels* 31 (9):10144–57. doi: 10.1021/acs.energyfuels.7b01666.

Turns, S. R. 1996. *An introduction to combustion*. New York, USA: McGraw-Hill Companies.

Wang, G., and J. Mi. 2018. What differences does large eddy simulation find among traditional, high-temperature, and moderate or intense low oxygen dilution combustion processes of a CH4/H2 jet flame in hot oxidizer coflow? *Energy Fuels* 32 (4):5544–58. doi: 10.1021/acs.energyfuels.7b03874.

Wang, L., Z. Liu, S. Chen, and C. Zheng. 2012. Comparison of different global combustion mechanisms under hot and diluted oxidation conditions. *Combustion Science and Technology* 184 (2):259–76. doi: 10.1080/00102202.2011.635612.

Westbrook, C. K., and F. L. Dryer. 1981. Simplified reaction mechanisms for the oxidation of hydrocarbon Fuels in flames. *Combustion Science and Technology* 27 (1–2):31–43. doi: 10.1080/00102208108946970.

Xiong, M., D. Liu, X. Chen, J. Ma, and L. Ma. 2020. Characteristics of a methane jet flame in elevated pressure and oxy-fuel atmosphere using large eddy simulation with tabulated chemistry. *Combustion Science and Technology* 194 (4):700–20. doi: 10.1080/00102202.2020.1780217.

Xu, S., Y. Chen, Z. Tian, and H. Liu. 2024. NO emission reduction characteristics of CH4/H2 staged MILD combustion over a wide range of hydrogen-blending ratios. *Fuel* 372:132239. doi: 10.1016/j.fuel.2024.132239.

Zhang, S., L. Zhang, P. Fu, H. Zhou, L. Hou, and Z. Ren. 2023. LES Investigation of kerosene spray flame emission characteristics in a staged combustor. *Combustion Science and Technology* 196 (17):4942–65. doi: 10.1080/00102202.2023.2240484.

Zivkovic, D., and T. Sattelmayer. 2023. Fractal based, scale-adaptive closure model for darrieus–landau instability effects on large-scale hydrogen-air flames. *Combustion Science and Technology* 195 (7):1573–98. doi: 10.1080/00102202.2023.2182201.